Journal of Applied Physics

Deal–Grove-like thermal oxidation of Si (001) buried under a thin layer of $SrTiO_3$

Cite as: J. Appl. Phys. **127**, 055302 (2020); https://doi.org/10.1063/1.5097839
Submitted: 28 March 2019 . Accepted: 19 January 2020 . Published Online: 04 February 2020

Wei Guo, A. B. Posadas, and A. A. Demkov

Journal of Applied Physics ARTICLE scitation.org/journal/jap

Deal–Grove-like thermal oxidation of Si (001) buried under a thin layer of $SrTiO_3$

Cite as: J. Appl. Phys. **127**, 055302 (2020); doi: 10.1063/1.5097839
Submitted: 28 March 2019 · Accepted: 19 January 2020 ·
Published Online: 4 February 2020

Wei Guo, A. B. Posadas, and A. A. Demkov[a)]

AFFILIATIONS

Department of Physics, The University of Texas, Austin, Texas 78712, USA

[a)]**Author to whom correspondence should be addressed:** demkov@physics.utexas.edu

ABSTRACT

Dry oxidation of Si (001) beneath a thin epitaxial $SrTiO_3$ layer has been studied using furnace annealing in flowing oxygen. A 10-nm layer of $SrTiO_3$ is epitaxially grown on Si with no SiO_2 interlayer. For such a structure, an annealing temperature of 800 °C was found to be the limiting temperature to prevent silicate formation and disruption of the interface structure. The effect of annealing time on the thickness of the SiO_2 layer was investigated. *In situ* x-ray photoelectron spectroscopy and reflection-high-energy electron diffraction were used to ensure that the quality of $SrTiO_3$ is unchanged after the annealing process. The experimental annealing data are compared with a theoretical oxygen diffusion model based on that of Deal, Grove, and Massoud. The model fits the experimental data well, indicating that oxygen diffusion through the $SrTiO_3$ layer is not the limiting factor. One can therefore readily control the thickness of the SiO_2 interlayer by simply controlling the annealing time in flowing oxygen.

I. INTRODUCTION

$SrTiO_3$ (STO) is a widely used substrate for metal oxide thin film growth.[1,2] It has a rather large dielectric constant (~300)[2] making it attractive for dielectric applications. The lattice constant of STO (3.9 Å) also makes it a suitable substrate material for the epitaxtial growth of many oxides with perovskite, rocksalt, and spinel crystal structures because of the small lattice mismatch to many such materials, such as $LaAlO_3$,[2–4] $BaTiO_3$,[5–7] EuO,[8,9] γ-Al_2O_3,[10] etc. The discovery by Mckee *et al.* in 1998 that one can epitaxially nucleate STO on Si directly without forming SiO_2 has opened epitaxial oxide thin films to the potential for technological development.[11] This process has been further developed and studied both experimetally and theoretically by several groups.[11–14] Even though STO has excellent dielectric properties making it attractive for use as a gate oxide in field effect transistors,[15] the conduction band offset at the STO/Si interface is essentially zero making such an application moot.[16,17] However, STO on Si can serve as a bridge material for integrating other oxides epitaxially on Si by serving as a pseudosubstrate.[6,7,9,14] It is therefore important to understand the behavior of this system under various temperature and oxygen pressure environments, particularly with respect to the oxidation of the underlying Si.

Silicon oxidation is a well-studied process that has been long-discussed following the establishment by Deal and Grove of the oxygen diffusion model for the Si surface in 1965.[18] This oxygen diffusion and reaction model of Si oxidation agrees well with the experimental data at different temperatures for relatively thick SiO_2 layers (>50 nm). The Deal–Grove model predicts the resulting oxide thickness for a given temperature as a function of time. However, significant deviations were found for thinner oxide films. Massoud improved the Deal–Grove model for the thin SiO_2 layer regime by adding an exponential decay term to the original linear-parabolic model.[19–21] Owing to the good dielectric properties of SiO_2 and a well-behaved Si–SiO_2 interface, controlled oxidation of Si has played a fundamental role in the fabrication of Si devices such as metal-oxide-semiconductor field-effect transistors (MOSFET) and single-electron devices.[22–26]

With epiaxial STO covering the Si surface, the oxidation behavior of Si may not be the same and it is important to know how the processing conditions, such as temperature and oxygen pressure, affect the oxidation rate of silicon with an STO overlayer present. A typical process of forming STO on Si involves first removing the surface SiO_2 and then depositing 0.5 monolayer (ML) of Sr in a molecular beam epitaxy (MBE) chamber. This submonolayer Sr prevents Si oxidation during the initial nucleation of

STO.[12,13] It is then followed by four to five unit cells (ucs) of STO deposition at low temperatures (<300 °C) which are then fully crystallized at ~500 °C. Once the initial template is crystallized, additional STO can be grown by treating the template as an STO substrate. Continuing the growth at oxygen pressures where STO is fully oxidized ($\sim 5 \times 10^{-7}$ Torr) and temperatures where STO is crystalline as deposited (~500 °C) typically results in some oxygen diffusing through STO and partially oxidizing the underlying Si. There have been several studies of Si oxidation and interlayer reaction at the STO/Si interface.[14,15,27] It has been shown that STO is not fully thermodynamically stable in direct contact with Si at very high temperatures under ultrahigh vacuum conditions.[28] Choi *et al.* grew STO/Si by MBE and used postdeposition anneal in oxygen (10^{-7}–10^{-5} Torr) to control the strain relaxation of STO.[14] Cross-section transmission electron microscopy (TEM) was used to monitor the interlayer structure and thickness under different oxygen partial pressures and annealing times. Goncharova *et al.* discussed the thermal stability of the STO/Si interface.[15] They considered the possible reactions that could happen between the layers at different annealing temperatures such as $STO + Si \rightarrow SiO + SrO + O_2 + TiSi_2$. A thin interlayer composed of $SrSiO_x$, SrO, and $TiSi_x$ was found at annealing temperatures as low as 550 °C. At 850 °C or even higher temperatures, the STO film decomposes completely, leaving behind only $TiSi_x$ islands.[29] Yong *et al.* have discussed the thermal stability and possible interface reactions of the STO/SiO_2/Si interface.[27] For example, $Si + SrTiO_3 \rightarrow SrSiO_3 + TiSi_2$ and $Si + TiO_2 \rightarrow SiO_2 + TiSi_2$. Optical microscopy and scanning electron microscopy (SEM) were used to observe the surface morphology changes of the STO film after annealing at ~800 °C. Eisenbeiser *et al.* used TEM to show the interfacial layer between STO and Si after the growth.[24]

Here, we study the dry oxidation behavior of the buried Si as a function of annealing time and determine the maximum temperature for which a relatively thin STO layer (10 nm) remains intact. STO is found to be stable during the oxidation anneal at 800 °C for up to 10 h. We start with the MBE growth of STO on Si (001) and then perform a flowing oxygen anneal in a tube furnace to oxidize the Si underneath. The STO thickness is fixed at 10 nm [25 unit cells (ucs)] for this study. Too thin STO layer (<10 uc) results in STO and Si reacting. The practical annealing temperature is found to be 800 °C. Below this temperature, dry oxidation is very slow and impractical; above this temperature, the STO in contact with Si is not thermally stable. We developed a theoretical model based on a modification of the Deal–Grove–Massoud formalism that predicts the thickness of SiO_2 formed underneath STO as a function of time and temperature and report a robust recipe for dry oxidation of Si buried under an epitaxial layer of STO.

II. EXPERIMENTAL

The STO/Si growth is performed in a customized DCA 600 MBE system with a base pressure of 6×10^{-10} Torr. P-type doped Si substrates of 20×20 mm^2 size are cut from a prime Si wafer and degreased ultrasonically in acetone, isopropanol, and de-ionized (18 MΩ/cm) water for 5 min each and then exposed to UV/ozone to remove carbon from the surface. The Si substrates are then annealed in ultrahigh vacuum at 700 °C for 10 min followed by Sr-assisted deoxidation before the growth of a 2-nm-thick STO epitaxial film.[11–14] Prior to the growth of STO, 1/2 ML of Sr is formed on the Si (001) surface. This Zintl layer has a 2×1 symmetry and serves as a template for further deposition.[11] The initially amorphous STO film is formed by codeposition of Sr and Ti at low temperatures (200 °C) under low oxygen pressures (8×10^{-8}–5×10^{-7} Torr) and is annealed in vacuum at or above 550 °C to crystallize. This procedure results in no interfacial SiO_2 as shown by x-ray photoemission and transmission electron microscopy.[12] There are two possible ways of growing additional STO. The first one is to deposit additional amorphous STO near room temperature in oxygen and anneal it in vacuum to the STO crystallization temperature (550 °C). This will not result in the formation of the SiO_2 interlayer. Another way is to perform codeposition of Sr and Ti under modest oxygen pressure (~mid 10^{-7} Torr) at 550 °C[14] (as if growing on an STO substrate). Because of the high oxygen diffusivity in STO, oxygen can diffuse through and oxidize Si underneath without disrupting the crystal structure of the already crystallized STO. This results in a very thin SiO_2 layer (~2 nm) between STO and Si. In this study, we use the first method to prepare an SiO_2-free interface prior to annealing. Reflection-high-energy electron diffraction (RHEED) with 21 keV electrons is used to record the STO crystallinity during growth. *In situ* x-ray photoelectron spectroscopy (XPS) using monochromated Al Kα radiation and a VG Scienta R3000 hemispherical electron energy analyzer is used to check stoichiometry of STO. The STO/SiO_2/Si samples are then measured using a J. A. Woollam M-2000DI spectroscopic ellipsometer to determine the thickness of SiO_2. The instrument uses a combination deuterium/quartz tungsten halogen lamp as the light source and covers a wavelength range from 190 to 1650 nm. The data are collected at three different angles of incidence (45°, 50°, and 55°). The fit is performed using the built-in software, CompleteEase, with three layers (Si substrate, thermal oxide SiO_2, and bulk $SrTiO_3$) over the entire wavelength range of the instrument. For the bulk $SrTiO_3$ optical constants, we use the parametrized optical constants determined by the Zollner group at the New Mexico State University.[30] All three angles of incidence are fit simultaneously using N, C, and S fit weighting. We show an example of a fit of the ellipsometry data in Fig. 1. The measured data are shown as circles and the fit curves as solid lines. The red one is the Ψ curve and the blue one is the Δ curve.

After a 10 nm-thick STO layer is grown in the MBE system [RHEED is shown in Fig. 2(a)], the sample is taken out of UHV and ultrasonically cleaned by IPA and DI water and inserted into a GSL-1700X-S tube furnace from MTI Corporation. Dry oxygen flows through the furnace tube during the entire annealing cycle with approximately 1 l/min flow rate at atmospheric pressure. We use dry oxidation to avoid a possible reaction between STO and water.[31] STO/Si samples are placed in the center of the furnace tube with the STO side facing up. The tube is heated gradually from room temperature to the final temperature at 10°/min. The sample is kept at this temperature for the designated period of time after which the sample is then cooled to room temperature over a period of 2 h. We verified that the STO film still has good crystallinity after the annealing by RHEED, which is shown in Fig. 2(b). To check the interface composition, we grew a relatively thin STO/Si sample with 5 nm of STO and checked it with XPS. The Si

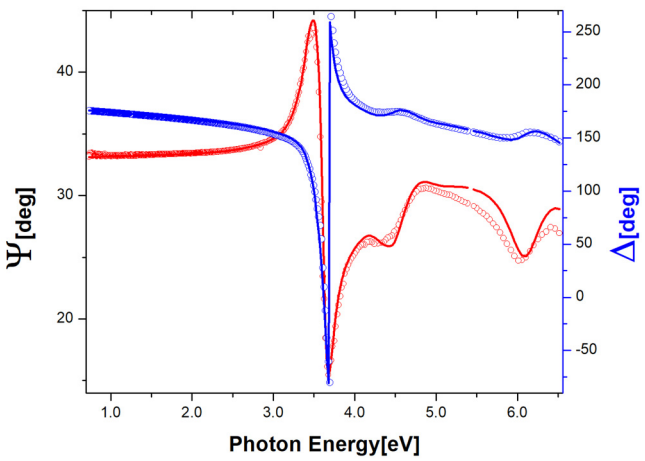

FIG. 1. Example ellipsometry measurement with the corresponding model fit. This is the measurement results at 45°. This gives a STO layer with 17.54 nm and a SiO_2 layer with 7.54 nm. The red one is the Ψ curve and the blue one is the Δ curve. Measured data are shown as circles and the fit curves as solid lines.

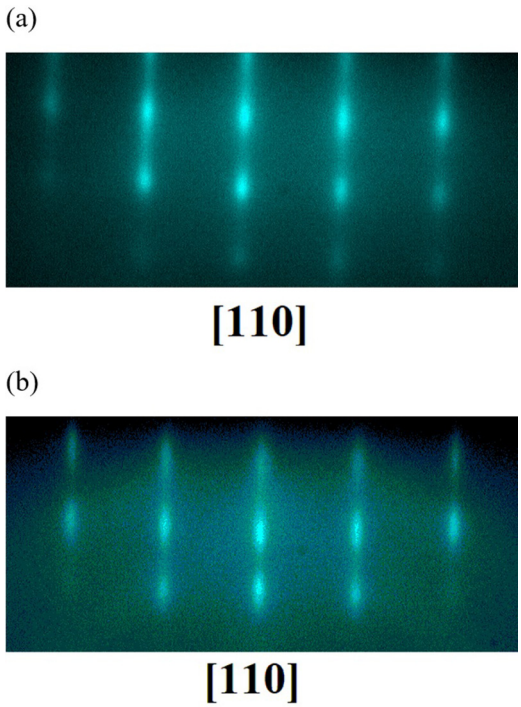

FIG. 2. (a) RHEED image for a 10 nm STO/SiO_2/Si after the growth and before anneal. The STO pattern is along [110]. (b) RHEED image for a 10 nm STO/SiO_2/Si after 800 °C anneal for 2 h. The STO pattern along [110] is still sharp and clear.

2p spectrum after the 800 °C anneal is shown in Fig. 3. It shows a major SiO_2 peak and a minor SiO_x peak, with no $TiSi_2$ signal visible.

It is known that it takes 15 h to grow a 10 nm-thick SiO_2 layer on bare Si[32] at 700 °C. The SiO_2 layer will grow more slowly at lower temperatures (<700 °C) because of the reduced oxygen diffusion rate. Most Si oxidation data in the literature are from the practically useful 800 °C–1300 °C temperature range. However, there are also papers reporting degradation of the STO/Si structure at high temperatures (~1000 °C) when STO reacts with SiO_2 and Si.[15,29] Therefore, the practical temperature range to have an acceptable oxidation rate without destroying STO is ~700–900 °C. The annealing temperature we use is 800 °C, which on the one hand is not high enough to degrade the STO layer but on the other hand, allows the Si oxidation time to remain practical. Under this annealing temperature, we compared the out-of-plane XRD full scan spectra before and after annealing for 4 h (Fig. 4). We find that the STO film only shows a little degradation, with the FWHM of the rocking curve of the STO (002) peak becoming slightly broadened from 0.33° to 0.54°.

III. THORETICAL MODEL

The standard model of Si oxidation has been proposed almost half a century ago by Deal and Grove.[18] It is based on describing three steps that result in oxidation: (i) oxygen (or oxidant species, in general) transport from the gas phase to the oxide surface where it is absorbed, (ii) oxygen transport through the oxide layer toward Si, and (iii) the interface oxygen reaction with Si and formation of a new layer of SiO_2. However, the model has a well-known difficulty in predicting the initial stage of oxidation for thin films. Massoud *et al.* made modifications to the Deal–Grove model to overcome this issue.[19–21] In the case where an STO overlayer is present, we have to modify the model further

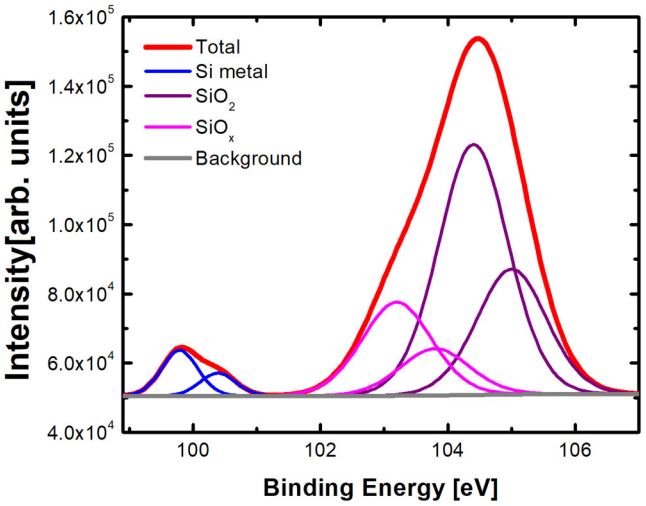

FIG. 3. XPS spectrum for the Si 2p region. The major peak is SiO_2 and the minor peak is SiO_x, Si metal is also still visible.

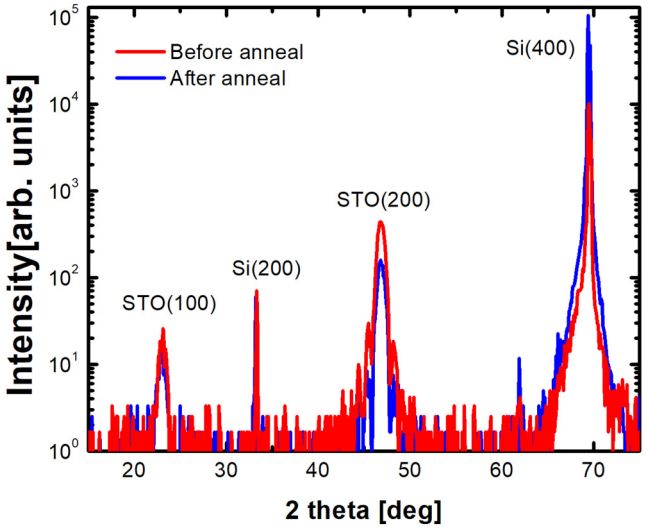

FIG. 4. Comparison of the XRD out-of-plane full scan of the before and after anneal sample. STO peaks decrease a little and Si is a little higher. All peaks have no obvious deformation.

as the initial oxide in our case is not SiO_2 but STO, and at later stages oxygen has to diffuse through both materials in order to reach Si.

Following the Deal–Grove–Massoud logic, we set the oxygen concentration in different regions and connect them by the oxygen diffusion flux. In Fig. 5, we show a schematic of the oxygen propagation through the structure. Here, C* is the oxygen

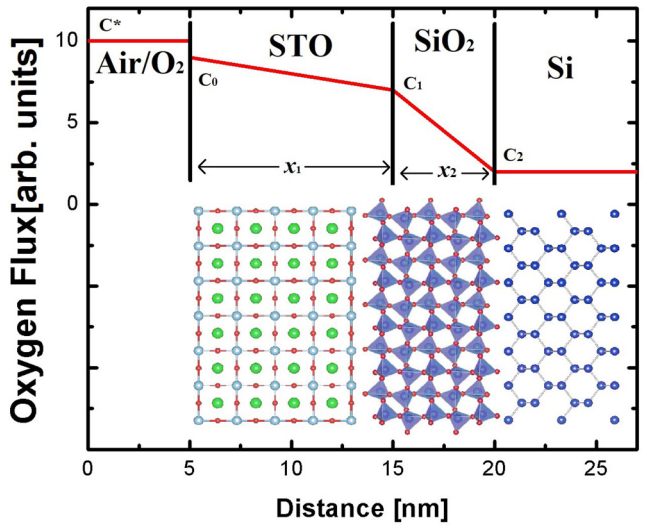

FIG. 5. The schematic of oxygen propagation in the $SrTiO_3/SiO_2/Si$ structure. The inset shows the atomic structure schematic.

concentration of the gas, C_0 is the oxygen concentration at the surface of STO, C_1 is the oxygen concentration at the STO/SiO_2 interface, and C_2 is the oxygen concentration at the SiO_2/Si interface. X_1 and x_2 are the thickness of STO and SiO_2, respectively. F_1 is the incoming oxygen flux, F_2 is the flux inside STO, F_3 is the flux inside SiO_2, and F_4 is the oxidation rate at the Si interface with SiO_2. The steady-state condition is discussed in the original paper.[18]

In the original Si oxidation model,[18] one has

$$F_1 = h(C^* - C_0), \tag{1}$$

where h is the transport coefficient (from gas into STO). The diffusion flux,

$$F_2 = -D_1 \frac{dC}{dx}, \tag{2}$$

is given by Fick's law, and because the gradient is linear, we have

$$F_2 = D_1 \frac{(C_0 - C_1)}{x_1}, \quad F_3 = D_2 \frac{(C_1 - C_2)}{x_2}, \quad F_4 = kC_2, \tag{3}$$

where D_1 is the diffusivity of oxygen in STO, D_2 is the diffusivity of oxygen in SiO_2, and k is the reaction rate of Si oxidation.

Since all fluxes are uniform, we set $F_1 = F_2 = F_3 = F_4$. Solving this system of equations, we obtain

$$\frac{C_0}{C^*} = \frac{1 + \frac{kx_1}{D_1} + \frac{kx_2}{D_2}}{1 + \frac{k}{h} + \frac{kx_1}{D_1} + \frac{kx_2}{D_2}}, \quad \frac{C_1}{C^*} = \frac{1 + \frac{kx_2}{D_2}}{1 + \frac{k}{h} + \frac{kx_1}{D_1} + \frac{kx_2}{D_2}},$$
$$\frac{C_2}{C^*} = \frac{1}{1 + \frac{k}{h} + \frac{kx_1}{D_1} + \frac{kx_2}{D_2}}. \tag{4}$$

The diffusivities of oxygen in STO and silica are compared in Fig. 6. We combine high temperature (>700 °C) diffusivity data of STO[33] from the literature and extrapolate to lower temperatures (300–700 °C) to find estimated diffusivities at those temperatures. One can see that in the temperature range from 300 °C to 1200 °C, oxygen diffusivity in STO, D_1, is always at least three orders of magnitude larger than that in silica, D_2. Thus, one can neglect the contribution coming from the term $\frac{kx_1}{D_1}$ in the following discussion. Therefore,

$$\frac{dx_2}{dt} = \frac{F}{N_1} = \frac{\frac{kC^*}{N_1}}{1 + \frac{k}{h} + \frac{kx_2}{D_2}} = \frac{B}{A + 2x_2}, \tag{5}$$

where N_1 here is the oxygen needed to oxidize a unit volume of Si, and A and B are defined as

$$A = 2D_2\left(\frac{1}{k} + \frac{1}{h}\right), \quad B = 2\frac{C^* D_2}{N_1}. \tag{6}$$

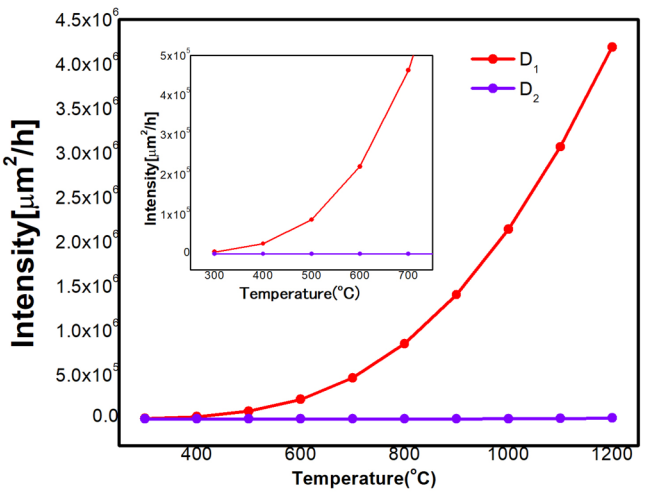

FIG. 6. Diffusivity of oxygen in $SrTiO_3$ (D_1) and SiO_2 (D_2) in the 300–1200 °C temperature range. The inset shows the diffusivity of oxygen in $SrTiO_3$ and SiO_2 in the 300–700 °C temperature range. The STO low temperature (<700 °C) data are obtained by the inverse relationship projection from the existing diffusivity at higher temperatures (>700 °C).

After the modifications of the Massoud model,[19,20]

$$\frac{dx_0}{dt} = \frac{B}{A + 2x_0} + C_1 e^{-x_0/L_1} + C_2 e^{-x_0/L_2}, \tag{7}$$

where A, B, C_i, and L_i can be fitted from the experimental values and are listed in the paper by Massoud *et al.*[19,20]

The steady-state picture can be justified as follows. Consider a sudden change in oxygen concentration in the silica layer, the total time it takes for the concentration to come back to a stable value is Δt,

$$\Delta t = \frac{\text{total oxygen needed to come back to original concentration}}{\text{oxygen flux}}. \tag{8}$$

Assuming that the total amount of oxygen needed is the same as the amount of oxygen that must flow out of the layer, the numerator is simply $\frac{1}{2}(C_1 - C_2)x_2$, and the flux oxygen flux is $F = D_2 \frac{(C_1 - C_2)}{x_2}$. Therefore,

$$\Delta t = \frac{\frac{1}{2}(C_1 - C_2)x_2}{D_2 \frac{(C_1 - C_2)}{x_2}} = \frac{x_2^2}{2D_2}. \tag{9}$$

Here, x_2 is on the order of nm and D is on the order of $\sim 10^8$ nm^2/h, so Δt is of the order of 10^{-8} h. Thus, we can assume that the flow of oxygen through the layer is established very quickly and can be assumed to be steady for all practical experimental conditions.

This suggests that we can treat the problem as the oxidation of bare Si since STO is essentially transparent to oxygen diffusion compared to SiO_2. Using the Massoud model,[20,21] we have

$$\frac{dx_0}{dt} = \frac{B}{A + 2x_0} + C_1 e^{-x_0/L_1} + C_2 e^{-x_0/L_2}. \tag{10}$$

Comparing with the experimental data, the formula can be rewritten as

$$\frac{dx_0}{dt} = \frac{B + K_1 e^{-t/\tau_1} + K_2 e^{-t/\tau_2}}{A + 2x_0}. \tag{11}$$

Solving this differential equation, we obtain

$$x_0 = \frac{A}{2} + \sqrt{\left(\frac{A}{2}\right)^2 + Bt + M_1\left[1 - \exp\left(-\frac{t}{\tau_1}\right)\right] + M_2\left[1 - \exp\left(-\frac{t}{\tau_2}\right) + M_0\right]},$$
$$M_0 = x_i^2 + Ax_i, \quad M_1 = K_1\tau_1, \quad M_2 = K_2\tau_2, \tag{12}$$

where x_i is the initial thickness of SiO_2, with the parameters given by

$$B = C_B \exp\left(-\frac{E_B}{kT}\right), \quad \frac{B}{A} = C_{B/A}\exp\left(-\frac{E_{B/A}}{kT}\right),$$
$$K_1 = K_1^0 \exp\left(-\frac{E_{K_1}}{kT}\right), \quad K_2 = K_2^0 \exp\left(-\frac{E_{K_2}}{kT}\right), \tag{13}$$
$$\tau_1 = \tau_1^0 \exp\left(\frac{E_{\tau_1}}{kT}\right), \quad \tau_2 = \tau_2^0 \exp\left(\frac{E_{\tau_2}}{kT}\right).$$

The constants are taken from Massoud[21] and are listed in Table I for convenience.

Based on these parameters in (12) and (13), we can estimate the silica thickness (x_0) for a given set of annealing time and temperature. We plot the silica thickness as a function of oxidation time at different temperatures in Fig. 7. The red diamond shapes in

TABLE I. Oxidation parameters of the Massoud model[21] for temperatures less than 1000 °C.

Crystal orientation	(100)	(111)	(110)
C_B (nm^2/min)	1.70×10^{11}	1.34×10^{9}	3.73×10^{8}
E_B (eV)	2.22	1.71	1.63
$C_{B/A}$ (nm/min)	7.35×10^{6}	1.32×10^{7}	4.73×10^{8}
$E_{B/A}$ (eV)	1.76	1.74	2.10
K_1^0 (nm^2/min)	2.49×10^{11}	2.70×10^{19}	4.07×10^{8}
E_{K_1} (eV)	2.18	1.74	1.54
K_2^0 (nm^2/min)	3.72×10^{11}	1.33×10^{9}	1.20×10^{8}
E_{K_2} (eV)	2.28	1.76	1.56
τ_1^0 (min)	4.14×10^{-6}	1.72×10^{-6}	5.38×10^{-9}
E_{τ_1} (eV)	1.38	1.45	2.02
τ_2^0 (min)	2.71×10^{-7}	1.56×10^{-7}	1.63×10^{-8}
E_{τ_2} (eV)	1.88	1.90	2.12

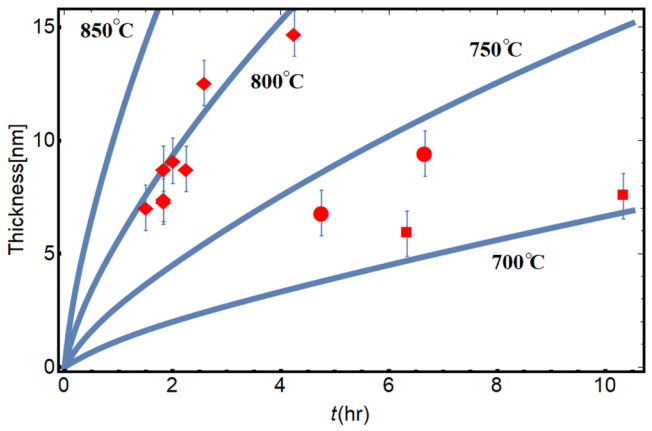

FIG. 7. The SiO_2 thickness as a function of oxidation time at different temperatures from Eqs. (12) and (13). The lines represent the model and the shapes represent the experimental data. Diamonds are samples annealed under 800 °C, circles under 750 °C, and squares under 700 °C. All with an error bar of 1 nm.

Fig. 7 are the experimental values from the tube furnace oxidation at 800 °C measured by ellipsometry. We also performed experiments at 750 °C and 700 °C to verify the prediction of the model for other temperatures. We want to emphasize that the model described above is derived based on the Deal–Grove–Massoud model using established parameters appropriate for Si/SiO_2 with no adjustable parameters. We use these established parameters to compare the model to the measured interfacial SiO_2 thicknesses and find reasonable agreement between the model predictions and the data, especially at 800 °C, with somewhat worse fits for the lower temperatures measured.

The uncertainty in the SiO_2 thickness comes from the particulars of the fitting of the ellipsometry data and the fluctuations present in the annealing process, particularly the oxygen flow rate. The fluctuations of the oxygen flow rate were found to cause drifts in the surface temperature of the sample resulting in oxidation thickness variations. We performed three anneals with the same condition and measured the SiO_2 thickness of each. The samples have the same structure before annealing and we controlled the oxygen flux at the same level. From this, we determine the random error in the SiO_2 thickness under 800 °C from the oxidation process to be 0.8 nm. Additionally, there is uncertainty due to the particulars of the ellipsometry fitting of up to 1 nm due to different wavelength ranges of fitting and different fit weighting. By choosing proper parameters, the error from the data fitting can be reduced to 0.1–0.2 nm. From this, we set the error bar in our plot to be 1 nm. Lower temperatures (under 800 °C) and longer anneal times (>1 h) would be expected to result in slightly larger errors as a result of the accumulation of uncertainty from the temperature variation due to the fluctuation in the oxygen flow rate. This could explain why the model works well for 800 °C and not so well for the lower temperatures.

At 800 °C, the oxidation rate is not prohibitively slow, while the temperature would not cause STO and Si to react and form $SrSiO_3$ or $TiSi_2$ as has been previously reported.[15,29,30] The data agree reasonably well with the model, indicating that one can estimate the dry oxidation time needed to obtain a desired thickness of SiO_2 while maintaining a thin single crystal STO film on top. We have explored temperatures higher than 800 °C in the range of 900–1200 °C. Unfortunately, at these higher temperatures, the STO layer breaks up and reacts with the Si substrate. However, dry oxidation at 800 °C is a robust method to produce interfacial SiO_2 layers in the thickness range of 10–50 nm. We have also explored other STO thicknesses (5, 20, and 40 nm) and have found that the STO film thickness does not matter if the STO thickness remains under 100 nm. This is confirmed by the model that shows that STO thickness is not important over a wide range of values.

IV. CONCLUSIONS

We studied the dry oxidation of STO/Si heterostructures and have demonstrated that the underlying Si can be safely oxidized at a relatively high temperature (800 °C) without significantly degrading the STO crystallinity. We deposited 10-nm of epitaxial STO on Si and performed flowing oxygen annealing at 800°C. The SiO_2 thickness is measured by ellipsometry and compared with our Deal–Grove-like oxidation model and is found to be in good agreement between the data and the model. We can use this model to predict the temperature and time needed to obtain the desired SiO_2 thickness for Si that is covered by a thin layer of STO. This additional knob for controlling the layer structure can enable one to integrate more complicated oxide structures on this STO/Si pseudosubstrate, especially for applications requiring complete decoupling between the STO and Si.

ACKNOWLEDGMENTS

This research was partially supported by the National Science Foundation (NSF) through the Center for Dynamics and Control of Materials: an NSF MRSEC under Cooperative Agreement No. DMR-1720595 and by the Air Force Office of Scientific Research (AFOSR) under Grant No. FA9550-18-1-0053.

REFERENCES

[1]B. Reihl, J. G. Bednorz, K. A. Müller, Y. Jugnet, G. Landgren, and J. F. Morar, Phys. Rev. B **30**, 803 (1984).
[2]A. A. Demkov and A. B. Posadas, *Integration of Functional Oxides with Semiconductors* (Springer, New York, 2014).
[3]J. E. Ortmann, N. Nookala, Q. He, L. Gao, C. Lin, A. B. Posadas, A. Y. Borisevich, M. A. Belkin, and A. A. Demkov, ACS Nano **12**, 7682 (2018).
[4]J. E. Ortmann, A. B. Posadas, and A. A. Demkov, J. Appl. Phys. **124**, 015301 (2018).
[5]P. Ponath, A. B. Posadas, M. Schmidt, A.-M. Kelleher, M. White, D. O'Connell, P. Hurley, R. Duffy, and A. A. Demkov, J. Vac. Sci. Technol. B **36**, 031206 (2018).
[6]K. D. Fredrickson, V. V. Vogler-Neuling, K. J. Kormondy, D. Caimi, F. Eltes, M. Sousa, J. Fompeyrine, S. Abel, and A. A. Demkov, Phys. Rev. B **98**, 075136 (2018).
[7]K. J. Kormondy, Y. Popoff, M. Sousa, F. Eltes, D. Caimi, M. D. Rossell, M. Fiebig, P. Hoffmann, C. Marchiori, M. Reinke, M. Trassin, A. A. Demkov, J. Fompeyrine, and S. Abel, Nanotechnology **28**, 075706 (2017).

[8]K. J. Kormondy, L. Gao, X. Li, S. Lu, A. B. Posadas, S. Shen, M. Tsoi, M. R. McCartney, D. J. Smith, J. Zhou, L. L. Lev, M. Husanu, V. N. Strocov, and A. A. Demkov, Sci. Rep. **8**, 7721 (2018).
[9]W. Guo, A. B. Posadas, S. Lu, D. J. Smith, and A. A. Demkov, J. Appl. Phys. **124**, 235301 (2018).
[10]K. Kormondy, A. Posadas, T. Q. Ngo, S. Lu, N. Goble, J. Jordan-Sweet, X. P. A. Guo, D. J. Smith, M. R. McCartney, J. G. Ekerdt, and A. A. Demkov, J. Appl. Phys. **117**, 095303 (2015).
[11]R. A. McKee, F. J. Walker, and M. F. Chisholm, Phys. Rev. Lett. **81**, 3014 (1998).
[12]H. Li, X. Hu, Y. Wei, Z. Yu, X. Zhang, R. Droopad, A. A. Demkov, J. Edwards, Jr., K. Moore, W. Ooms, J. Kulik, and P. Fejes, J. Appl. Phys. **93**, 4521 (2003).
[13]Y. Wei, X. Hu, Y. Liang, D. C. Jordan, B. Craigo, R. Droopad, Z. Yu, A. Demkov, J. John, L. Edwards, and W. J. Ooms, J. Vac. Sci. Technol. B **20**, 1402 (2002).
[14]M. Choi, A. B. Posadas, R. Dargis, C. K. Shih, A. A. Demkov, D. H. Triyoso, N. David Theodore, C. Dubourdieu, J. Bruley, and J. Jordan-Sweet, J. Appl. Phys. **111**, 064112 (2012).
[15]L. V. Goncharova, D. G. Starodub, E. Garfunkel, T. Gustafsson, V. Vaithyanathan, J. Lettieri, and D. G. Schlom, J. Appl. Phys. **100**, 014912 (2006).
[16]X. Zhang, A. A. Demkov, H. Li, X. Hu, Y. Wei, and J. Kulik, Phys. Rev. B **68**, 125323 (2003).
[17]F. Amy, A. S. Wan, A. Kahn, F. J. Walker, and R. A. McKee, J. Appl. Phys. **96**, 1635 (2004).
[18]B. E. Deal and A. S. Grove, J. Appl. Phys. **36**, 3770 (1965).
[19]H. Z. Massoud, J. D. Plummer, and E. A. Irene, J. Electrochem. Soc. **132**, 1745 (1985).
[20]H. Z. Massoud, J. D. Plummer, and E. A. Irene, J. Electrochem. Soc. **132**, 2693 (1985).
[21]H. Z. Massoud and J. D. Plummer, J. Appl. Phys. **62**, 3416 (1987).
[22]A. F. Tasch, T. C. Holloway, K. F. Lee, and J. F. Gibbons, Electron. Lett. **15**, 435 (1979).
[23]W. Hänsch, T. Vogelsand, R. Kircher, and M. Orlowski, Solid-State Electron. **32**, 839 (1989).
[24]K. Eisenbeiser, J. M. Finder, Z. Yu, J. Ramdani, J. A. Curless, J. A. Hallmark, R. Droopad, W. J. Ooms, L. Salem, S. Bradshaw, and C. D. Overgaard, Appl. Phys. Lett. **76**, 1324 (2000).
[25]S. Guha and V. Narayanan, Phys. Rev. Lett. **98**, 196101 (2007).
[26]J. W. Park, D. F. Bogorin, C. Cen, D. A. Felker, Y. Zhang, C. T. Nelson, C. W. Bark, C. M. Folkman, X. Q. Pan, M. S. Rzchowski, J. Levy, and C. B. Eom, Nat. Commun. **1**, 94 (2010).
[27]G. J. Yong, R. M. Kolagani, S. Adhikari, W. Vanderlinde, Y. Liang, K. Muramatsu, and S. Friedrich, J. Appl. Phys. **108**, 033502 (2010).
[28]K. J. Hubbard and D. G. Schlom, J. Mater. Res. **11**, 2757 (1996).
[29]A. Posadas, R. Dargis, M. Choi, A. Slepko, A. A. Demkov, J. J. Kim, and D. J. Smith, J. Vac. Sci. Technol. B **29**, 03C131 (2011).
[30]S. Zollner, A. A. Demkov, R. Liu, P. L. Fejes, R. B. Gregory, P. Alluri, J. Curless, Z. Yu, J. Ramdani, R. Droopad, T. E. Tiwald, J. N. Hilfiker, and J. A. Woollam, "Optical properties of bulk and thin-film SrTiO3 on Si and Pt," J. Vac. Sci. Technol. B **18**, 2242–2254 (2000).
[31]H. S. Kato, S. Shiraki, M. Nantoh, and M. Kawai, Surf. Sci. **544**, 722 (2003).
[32]See http://www.lelandstanfordjunior.com/thermaloxide.html for the time needed for 10 nm-thick SiO_2 thickness at 700 °C.
[33]P. Pasierb, S. Komornicki, and M. Rekas, J. Phys. Chem. Solid **60**, 1835 (1999).